Geomorphology 135 (2011) 108–116

Contents lists available at SciVerse ScienceDirect

Geomorphology

journal homepage: www.elsevier.com/locate/geomorph

Formation of the highest sand dunes on Earth

Xiaoping Yang [a,*], Louis Scuderi [b], Tao Liu [a], Philippe Paillou [c], Hongwei Li [a], Jufeng Dong [a], Bingqi Zhu [a], Weiwei Jiang [d], Andrew Jochems [b], Gary Weissmann [b]

[a] CAS (Chinese Academy of Sciences) Key Laboratory of Cenozoic Geology and Environment, Institute of Geology and Geophysics, CAS, P.O. Box 9825, Beijing 100029, China
[b] Department of Earth and Planetary Sciences, University of New Mexico, MSC03 2040, Albuquerque, NM 87131-1111, USA
[c] Université de Bordeaux, Observatoire Aquitain des Sciences de l'Univers, UMR 5804, LAB/UMR 5218, IMS, 2 rue de l'Observatoire, 33271 Floirac, France
[d] CAS Key Laboratory of Petroleum Geophysics, Institute of Geology and Geophysics, CAS, P.O. Box 9825, Beijing 100029, China

ARTICLE INFO

Article history:
Received 13 April 2011
Received in revised form 5 August 2011
Accepted 8 August 2011
Available online 16 August 2011

Keywords:
Dune formation
Aeolian process
Gravity method
Remote sensing
Climate change
China

ABSTRACT

Characterization of dune morphology has historically been based on relationships between dune forms and wind regimes with dune height shown to be sensitive to atmospheric boundary layer depth, sand availability and sediment properties. While these parameters have been used in numerical simulations to model the occurrences of some types of dunes, they cannot alone explain the great diversity in form and size seen on Earth and on other solar system bodies. Here we present results from our studies of dune formation in the Badain Jaran Desert in western China, where Earth's tallest dunes occur. We measured the variability of the dune morphology in this desert on the basis of LANDSAT ETM+ data, and we detected the bedrock landforms beneath the aeolian sands by applying gravity methods. Wind records from stations at the periphery of the desert and SRTM topographical data were examined also to augment the interpretation. Our studies demonstrate that in addition to average wind parameters, dune height is highly sensitive to local geology, subsurface characteristics, and topography, and interactions between changing climate conditions and aeolian and fluvial processes. These additional factors need to be considered in the interpretation and simulation of dunes on Earth. We anticipate that analysis of anomalous dune heights like those seen in the Badain Jaran may also provide critical information on subsurface characteristics and environmental conditions on Earth and on other planetary bodies.

1. Introduction

Dune form and size vary greatly globally and often differ significantly within a single desert (e.g., Fryberger and Dean, 1979; Lancaster, 1995; Goudie, 2002). Our understanding of dune morphology has largely been based on relationships between dune morphology and wind regimes (e.g., Bagnold, 1941; Fryberger and Dean, 1979; Zhu et al., 1981; Lancaster, 1995; Livingstone et al., 2006; Bullard and Livingstone, 2010). Dune height has been shown to be sensitive to atmospheric boundary layer depth (Andreotti et al., 2009), sediment availability (Kocurek and Lancaster, 1999), and sediment properties (Rubin and Hesp, 2009). While these parameters have been used in numerical simulations to model the occurrences of some types of dunes (e.g., Narteau et al., 2009; Parteli et al., 2009; Zhang et al., 2010; Delgado-Fernandez, 2011), the great diversity in dune form and size seen on Earth and on other solar system bodies remains poorly understood.

China's Badain Jaran Desert (Fig. 1) covers an area of ~49,000 km^2 and is characterized in its southern and southeastern parts by the occurrence of densely distributed giant dunes with heights commonly between 200 and 300 m with a maximum of 460 m. The mean annual precipitation decreases from ca. 120 mm in the southeast to ca. 40 mm in the northwestern margin of the desert. The mean annual evaporation is just ~1000 mm from the lake surface and ~100 mm from the land surface in the southeastern part of the sand sea according to more recent studies (Yang et al., 2010a), although much large values were reported earlier (e.g., Zhu et al., 1980). On the dune slopes there is a spare vegetation cover consisting of xerophilous grasses and shrubs with some plants like *Artemisia*, *Agriophyllum* and *Achnatherum* occurring even close to the ridges of the high dunes. Around the lakes and springs in the inter-dune depressions there are abundant grasses and shrubs used for animal grazing and for cooking fuel by the local residents.

The dunes in the Badain Jaran are mainly compound forms and dune chains, consisting of multiple dune generations arising from Quaternary climate changes (Yang et al., 2003), although simple giant dunes with obvious steep lees and relatively steep windward slopes occur as well (Yang, 1991). On the southeastern margin of the sand sea typical pyramid dunes are not rare (Zhu et al., 1980). The giant dunes, named also as compound, crescentic ridges (Breed and Grow, 1979), are the tallest dunes on Earth (e.g., Fryberger and Dean, 1979; Zhu et al., 1980; Yang, 1991; Jäkel, 1996; Yang et al., 2003, 2010a) and

* Corresponding author. Tel.: +86 10 8299 8387.
E-mail addresses: xpyang@263.net.cn, xpyang@mail.igcas.ac.cn (X. Yang).

0169-555X/$ – see front matter © 2011 Elsevier B.V. All rights reserved.
doi:10.1016/j.geomorph.2011.08.008

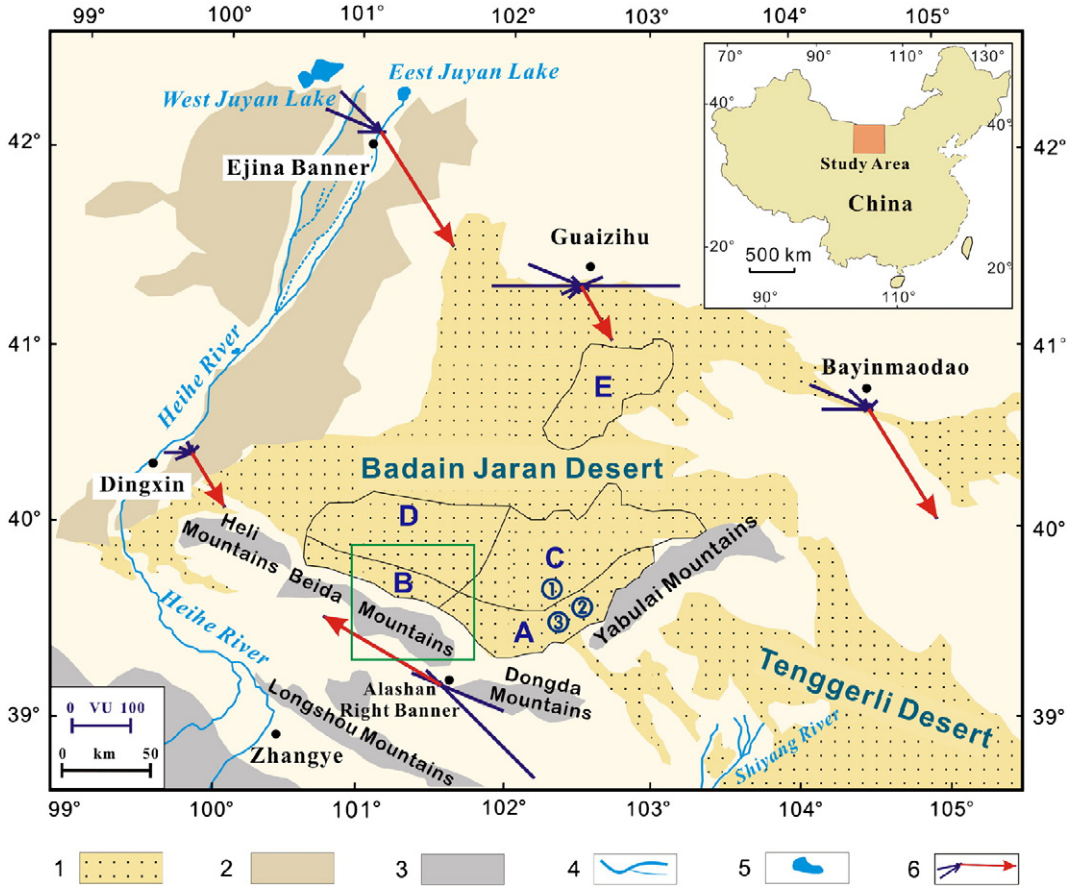

Fig. 1. Overview of the Badain Jaran desert. A, B, C, D and E designate areas used to map the dunes. Legend: 1, Sand dunes. 2, Fluvial sediments associated with the Heihe River. 3, Adjacent mountain ranges. 4, Rivers. 5, Lakes, and, 6, sand roses (Fryberger and Dean, 1979) for each of the five surrounding weather stations, with blue lines showing winds capable of transporting sand from various directions (DP) and red lines with arrows indicating the resultant sand transport trend (RDP). Numbers in circles show the locations of the dunes examined in great detail and the green square indicates the location of Fig. 8.

taller than all dunes so far found on other planetary bodies (Lancaster, 2006; Lorenz and Radebaugh, 2009; Zimbelman, 2010). Here we document the variation of dune morphology in this desert and the environmental and geologic conditions in which these anomalously high dunes formed. Our results provide insights into the giant dune formation processes that may be applicable in understanding dune formation in other regions on Earth and on other solar system bodies.

2. Methods

LANDSAT ETM+ data from 2001 and 2002 (30 m spatial resolution) was used to determine the lengths and crest strike of 1758 dunes in the areas where giant dunes occur in this sand sea (Fig. 1 and Table 1). Wind records covering the period from 1965 to 2004 from five stations at the periphery of the Badain Jaran were used to interpret the potential movement of sand. Sand drift potential (DP), resultant drift potential (RDP), the resultant direction of sand movement (RDD) and the directional variability (RDP/DP) were estimated following Fryberger and Dean (1979). Metric unit ($m\ s^{-1}$) of wind speed was used for calculations and their values were finally converted to vector units with the wind speed in knots (Bullard, 1997; Table **2**).

One of our major goals was to obtain a regional image of bedrock topography. Initially, we applied seismic and ground penetrating radar (GPR) in the study area but failed, because the aeolian sand is too thick for GPR to penetrate to the depth of bedrock in most cases, and the loss of seismic signals is too rapid in the aeolian sands for shallow-seismic approaches. Electromagnetic soundings were limited by the low conductivities of the dry sand layers on the surface. We however found that the gravity method (Dobrin, 1976) was the most promising, although we know of no earlier cases of mapping bedrock topography in sand seas using this method. Mapping of buried valleys (Lennox and Carlson, 1967), bedrock topography underlying moraines (Annecchione et al., 2001) as well as underground salt tectonics (Hamdi-Nasr et al., 2009), however, demonstrate the potential of this method in investigating sub-surface landforms. Since the bedrock and aeolian sand have different densities, and the denser rocks have a greater gravitational attraction, the depth of bedrock can therefore be calculated from gravity data.

Table 1
Variations of dune strikes and densities in the study area: percentage of dunes in each strike category by subdivision (see Fig. 1) and average length of the dune ridges (dune density) in the Badain Jaran Desert.

Strike	Area					
	A	B	C	D	E	Mean
E–W	0.4	0.0	0.6	0.0	0.0	0.3
NEE–SWW	3.6	2.3	7.9	9.9	2.4	5.4
NE–SW	56.1	45.5	67.9	62.9	38.0	58.0
NNE–SSW	37.6	46	22.7	25.6	52.2	33.6
N–S	1.2	5.2	0.2	1.6	6.8	1.9
NNW–SSE	0.6	0.7	0.0	0.0	0.6	0.3
NW–SE	0.3	0.2	0.0	0.0	0.0	0.1
NWW–SEE	0.3	0.0	0.7	0.0	0.0	0.4
Density ($m\ km^{-2}$)	439	249	235	89	137	207

Table 2
Sand drift potential (DP), resultant drift potential (RDP), the resultant direction of sand movement (RDD, 0 referring to the north, clockwise) and the directional variability (RDP/DP) based on wind records at the margins of the Badain Jaran Desert from 1964 to 2004 (vector units with wind speed in knots).

	Station				
	Alashan Right Banner	Bayinmaodao	Dingxin	Ejina Banner	Guaizihu
DP	457	335	178	281	595
RDP	228	214	106	227	105
RDD	300	148	149	148	150
RDP/DP	0.50	0.64	0.60	0.81	0.18

Gravity readings were taken with a LaCoste & Romberg G1168 gravimeter and station elevations and relative positions (distance and direction) were surveyed simultaneously using a GTS-100N total station. The precision of this gravity meter is ~0.01 milligal (mGal). To ensure the normal operation of the instrument the meter was tested at national base stations around Beijing shortly before being used in the Badain Jaran Desert. Measurements at the base stations near each dune were repeated as often as possible but minimum measurements were taken at the beginning and end of the day to correct for instrumental drift. The accuracy of the gravity readings was assured in the field by taking multiple observations at each station until satisfactory replication was obtained. Bedrock outcrops found in inter-dune areas were used as the base stations, with the reported gravity anomaly referring to the gravity difference between stations and their own reference datum after various corrections. Three different sites with compound dunes in the southeastern of the sand sea were selected for gravity measurements because of the availability of bedrock outcrops (as base stations) nearby and the sufficient height of the dunes (>200 m). Four major steps were used to correct the readings from the gravity meter:

A) Earth-tidal, instrumental drift and latitude corrections
The readings from the gravity meter were firstly corrected for Earth-tidal and instrumental drift, and latitude changes (Dobrin, 1976). Instrumental drift was based on our field records, and the latitude corrections were realized by precisely measuring the relative displacement of the measurement stations in the north–south direction. The gravity formula for the variation of standard gravity along the geoid with the latitude ϕ (degrees) is (Burger et al., 2006):

$$g\,[\mathrm{Gals}] = 978.03185\left(1 + 0.005278895\,sin^2\phi + 0.000023462\,sin^4\phi\right) \quad (1)$$

For our transects the variation is 0.1 milligal (10^{-3} Gal) for each 124.85 m of displacement in the north–south direction. The values for Earth-tidal corrections for our transects were provided by the Institute of Geophysics, China Earthquake Administration with consideration to exact coordinates of the study sites and precise timing of the measurements.

B) Terrain corrections
The corrections take into account the undulations of topography above and below the elevation of the observation station, and were implemented manually following the charts and tables of Hammer (1939). A portion of the correction was determined in the field on the basis of the local slopes and form of the terrain and the remainder of the correction was calculated from topographic maps. Hammer's method considers the gravity effect of a ring, as follows:

$$\Delta g\,[\mathrm{Gals}] = 2\pi G\sigma n^{-1}\left[R_o - R_i + \left(R_i^2 + z^2\right)^{\frac{1}{2}} - \left(R_o^2 + z^2\right)^{\frac{1}{2}}\right] \quad (2)$$

where G is the universal gravitation constant (6.67384×10^{-11} m^3 kg^{-1} s^{-2}), σ is the density of the mass (kg m^{-3}), z is the thickness of the ring (m), R_o is its outer radius (m) and R_i (m) inner radius, and n is the number of sectors by that the ring is divided. All sector effects were calculated individually and finally added together to the observed gravity.

C) Elevation corrections
Because gravity decreases 0.3086 mGal for every meter above sea level, the following equation is used for elevation corrections (Burger et al., 2006):

$$\Delta g\,[\mathrm{mGal}] = -0.3086h \quad (3)$$

where h is the elevation difference (m) above the datum of each transect.

D) Free-air corrections
The corrections take into the impact of the mass between the observation point and the datum. As the radius of this mass is usually much larger than its thickness,

$$\Delta g\,[\mathrm{mGal}] = 0.04193\sigma h \quad (4)$$

These corrections are added as long as the mass is above the datum and subtracted if it is below the datum (Dobrin, 1976; Burger et al., 2006).

A reduction density of 1.6 g cm^{-3} (the mean density of aeolian sand in this sand sea) and the base station reference were used for these corrections in each case. The final gravity anomaly values indicate the change in the pull of gravity along the traverses crossing each dune.

For the simulation of the underground topography we assumed a constant density contrast between the bedrock and the aeolian sediment. The difference in density between aeolian sand and the bedrock is a key factor impacting the interpretation of the bedrock occurrence at each point of the survey. The average density of aeolian sands in the dunes we studied is 1.6 g cm^{-3}, and those of granites and conglomerates are 2.6 and 2.4 g cm^{-3}, respectively, according to our laboratory experiments. Thus, the aeolian sand and bedrock density differences are 1.0 and 0.8 g cm^{-3}, respectively. To quantitatively detect the boundary between the bedrock and the aeolian sand, forward gravity modeling was performed using the software program Mask 2000 (Yao, 2009). Normally, gravity modeling suffers from non-uniqueness. The interpretation of the finally corrected anomaly values was constrained by the observations at exposed outcrops.

To augment this geophysical modeling approach we also extracted the elevation of each interdune depression using SRTM data (90 m grid cell resolution and augmented by Google Earth™) and produced an interpolated profile that revealed the general trend and slope of subsurface features.

3. Results and discussion

Variability in dune morphology in the Badain Jaran Desert is reflected in the regional differences in dune size, strike and density (average dune ridge length in a given area). The longest is 7.5 km and the shortest is <1 km (maximum error ~60 m). Dune density varies distinctly across the entire study area, between 439 m km^{-2} in the southeast (Area A in Fig. 1) and 89 m km^{-2} in the inner western section (Area D in Fig. 1) (Table 1). In Areas A, C and D the dunes strike predominately NE–SW; however, in Area B the percentage of dunes with NNE–SSW strikes is slightly higher than those trending NE–SW; and in Area E, more than half of the dunes strike NNE–SSW. This variability suggests potential control of the predominant dune strike by interactions between regional winds and blocking mountain ranges.

Sand roses (Fig. 1) show that directional variability differs greatly on the margins of the Badain Jaran, indicating the impact of regional topography and suggesting that the areas in the north (Guaizihu) and southwest (Alashan Right Banner) are high-energy environments while the west margin (Dingxin) is a low-energy environment. Under the control of the East Asian winter monsoon, northwest winds would be predominant without the strong impact of these local mountain ranges. Among the five stations, Guaizihu, which exhibits frequent changes in wind direction, is the site with the highest total DP and the lowest resultant RDP (Table **2**). The directional variability, RDP/DP, is classified as follows: low in Guaizihu, high in Ejina, and intermediate in other stations. Low RDP/DP is associated with complex wind regimes while high values are indicative of wide and narrow unimodal wind regimes (Table **2**).

Changes in the simple Bouguer gravity anomaly (Dobrin, 1976) along dune crossing traverses (Figs. 2 to 5) indicate that bedrock landforms form a basement under all four dunes surveyed with only one dune having a bedrock core directly under its ridge (Fig. 3). Our results suggest that giant dunes were built up when aeolian sands accumulated and grew on these gently sloping bedrock hills. A 250 m high dune located north of the bedrock hill in Fig. 2 (top) forms on the windward slope of the hill, and the form of the dune is similar to the bedrock relief. At most sites along the traverses the thickness of the aeolian sands reaches a maximum of ~200 m on the dune ridges. On the lower portions of the dune slopes, the thickness of aeolian sands is often less than 10 to 20 m.

The mapping of dune sand thickness via gravity methods is supported by our mapping of interdune elevations that are indicative of the groundwater table associated with the occurrence of interdune lakes (Yang et al., 2003, 2010a). The height distribution of interdune depressions should reflect the minimal elevations of the water table associated with the underlying bedrock (Fig. 6). This surface was subtracted from the surface DEM to estimate total sand depth and its distribution across the region containing the giant dunes (Fig. 7). We interpret this as representing the gently sloping surface of a former Distributive Fluvial System (DFS, Craddock et al., 2010; Weissmann et al., 2010) emanating from the southeast that was subsequently eroded into low rolling hills.

Earlier studies have attempted to explain the genesis of these globally tallest dunes from various perspectives. Chen et al. (2004) reported that the giant dunes were maintained by subsurface flow of groundwater from mountains of the northeastern Tibetan Plateau. Yang (1991) and Jäkel (1996) assumed that some dunes might have a bedrock core with the top of these bedrock hills often just beneath the dune ridges. The subsurface landforms, visualized for the first time on the basis of our gravity data and regional mapping of interdune elevations using SRTM data, suggest that a small percentage of the dunes have a bedrock hill directly beneath their ridgelines and that the subsurface is a subdued and dissected low-relief erosional surface (maximum relief ~100 m) sloping at a low angle towards the northwest. Compared with the elevation of the inter-dune depressions, the surface of this hilly bedrock raises the relative height of the dunes considerably (Figs. 2 and 3). In fact, the giant dunes only occur in the southeastern parts where the effects of the subsurface actually come into play. The dunes in the central and northern portion of the sand sea are subdued and somewhat disorganized probably due to locations distant from the mountain ranges (Fig. 1 and Table 1) and sand thickness decreases also (Fig. 7). This general trend of the sand thickness variation (Fig. 7) suggests that the seasonal changes of wind directions (Fig. 1) do not have an obvious impact on the size of the dunes, because tall dunes are not located in areas with large variability of wind directions, such as in Guaizihu.

Sand availability is another key component of the aeolian system in the Badain Jaran Desert. In addition to sand provided by the Hehei River in the northwest (Fig. 1), we have also found that the alluvial sediments deposited on the south and southeast margins of the desert are significant sand sources. Although the desert region is generally under the impact of prevailing northwest winds related to the East Asian monsoon system, precisely measured profiles crossing the dunes (Figs. 2 to 4) and wind data from local weather stations (Fig. 1) suggest that southeast winds are also important in shaping the dunes. The steep slopes in the northwestern side of the dunes (Figs. 2 to 4) demonstrate strong impact of southern and southeastern winds, meaning that the seasonal variation of winds plays a role in the shapes of dunes, even though there is no wind record directly from the dune areas (Fig. 1).

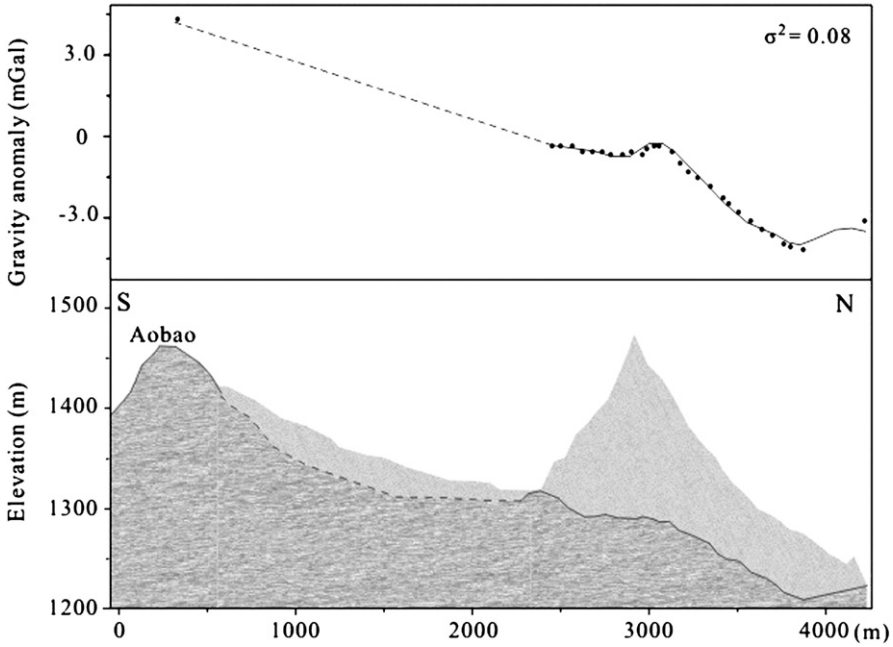

Fig. 2. Subsurface topography of location 1 in Fig. 1, interpreted from the gravity data, indicating an earlier stage of the formation of a tall dune. The bedrock hill (local name Aobao) consisting of conglomerates is still visible. Dots are the field measurements after corrections and the lines represent the results of the forward modeling.

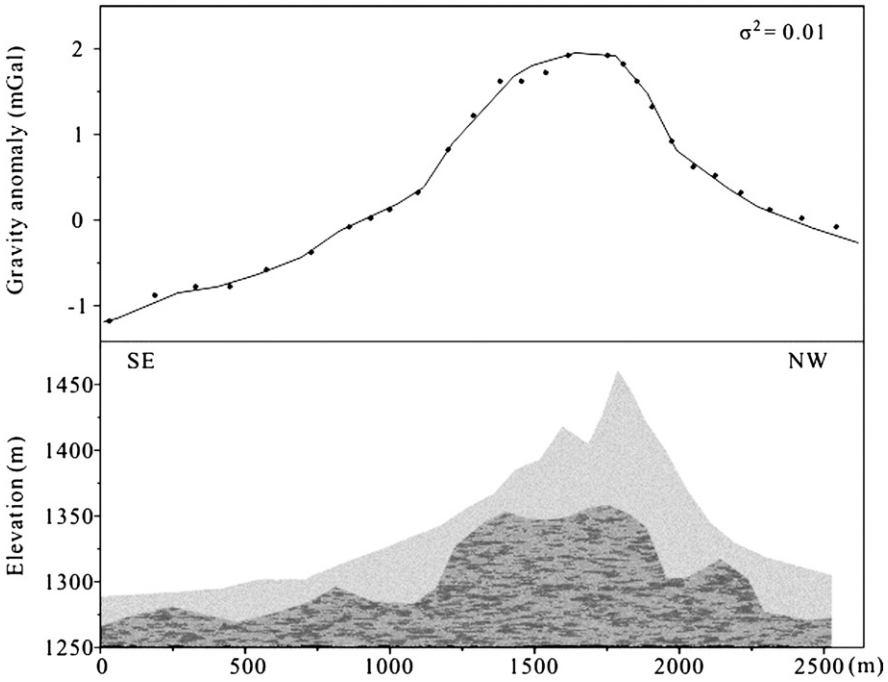

Fig. 3. Subsurface topography of location 2 in Fig. 1, interpreted from the gravity data. A bedrock hill (granite) has been fully covered by aeolian sand. Dots are the field measurements after corrections and the lines represent the results of the forward modeling.

Mapping of intermittent stream channels shows that sediments introduced by fluvial processes from the mountains on the Badain Jaran's southern margin are also direct sand sources for the dunes (Fig. 8). It is visible that the streams are able to penetrate deep into the dune fields (Fig. 8). Conglomerates found beneath these dunes (Figs. 2 and 4) are cemented alluvial deposits transported by water flowing from southern drainages during earlier periods of wetter climate. Similar conglomerates often occur beneath aeolian sands in the southern Badain Jaran, and are commonly encountered in this region while drilling wells for drinking. The age of these deposits needs to be determined in future studies.

Our gravity data offer a geophysical scanning of the internal structure of the tall dunes, making the deeply hidden boundary between the subsurface landforms and the thick aeolian sands visible. The relationship between bedrock and aeolian sands is complicated by the active and continuous movement of the sands under strong aeolian dynamics. Referring to the impact of subsurface geology on aeolian landforms, there is some similarity between desert dunes and hills covered by aeolian loess in the widest sense. As a matter of fact, the initial interpretation for the aeolian origin of loess in China was heavily based on the observation that loess appears in all kinds of landforms (Richthofen, 1877), and the morphology underneath the

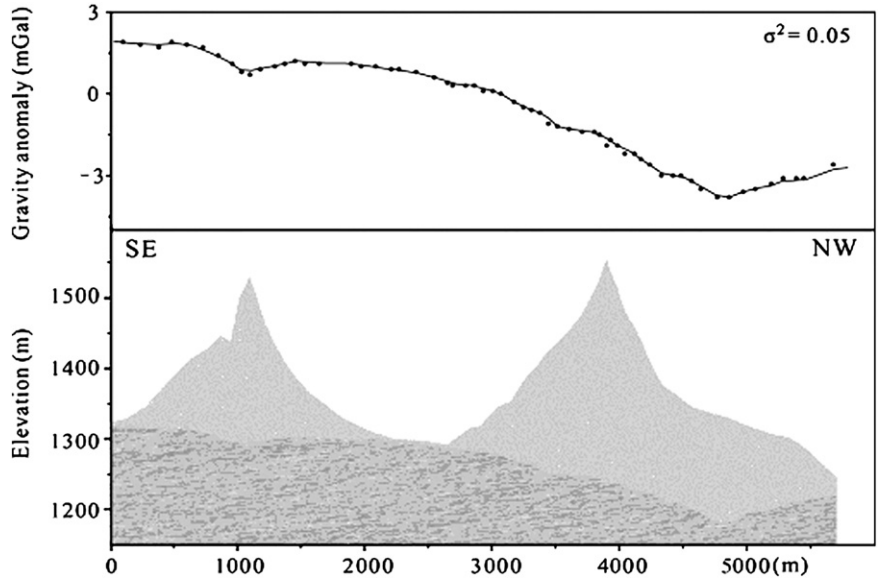

Fig. 4. Subsurface topography of location 3 in Fig. 1, interpreted from the gravity data. Compared to the inter-dune elevations, the bedrock slope consisting of conglomerates has raised the height of these two dunes considerably. Dots are the field measurements after corrections and the lines represent the computed gravities. Both windward and lee sides of the dune are steep due to strong winds from multiple directions (primarily NW and SE).

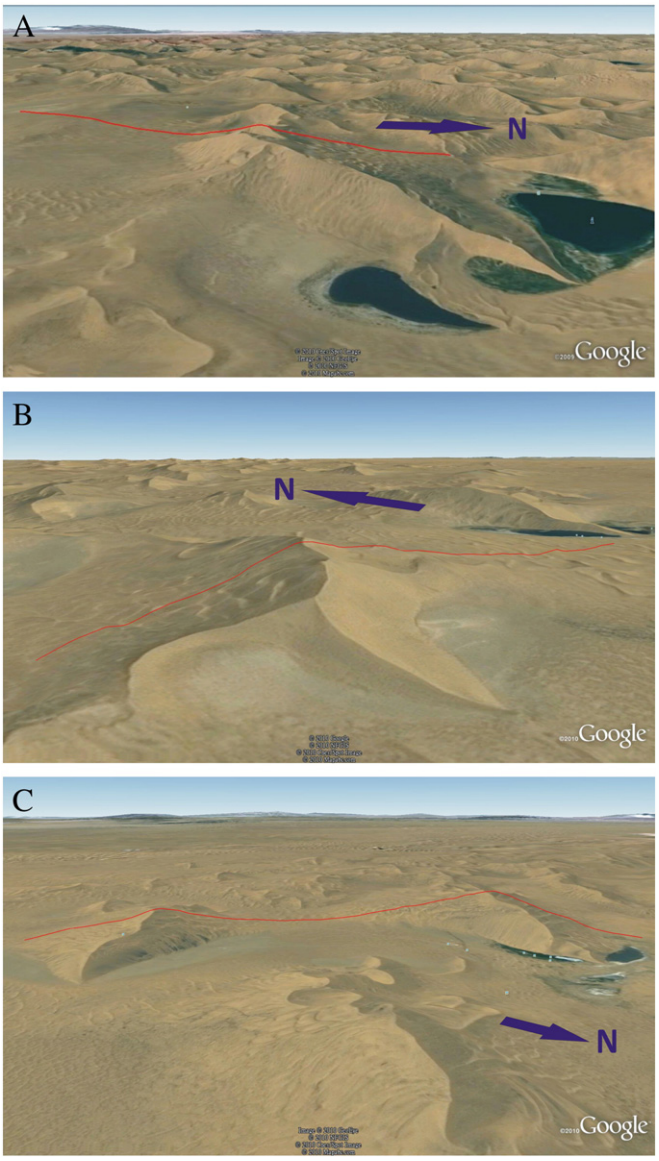

Fig. 5. Overview of the transects in 3-D Google Earth images. A) Location of the transect 1 (Fig. 2); B) location of the transect 2 (Fig. 3); C) location of the transect 3 (Fig. 4).

loess layer can be still seen in various gullies or vallies (Yang et al., 2010b). Of course the aeolian processes reshape the aeolian landscape tremendously like in the Badain Jaran, and it happens in the loess region even in Europe although to a much smaller extent (Goossens, 1997).

Alteration between arid and slightly wetter conditions during the Late Quaternary also contributes to the aggregation of the dunes in the Badain Jaran Desert. This climate variability results in calcareous cementation of many dune surfaces during periods of increased rainfall (Yang et al., 2003). Renewed formation of dunes on these older cemented surfaces substantially increases the height of these dunes. Similar dune height increasing mechanisms, i.e., via formation of stabilized surfaces by organic debris and palaeosols, have been suggested using GPR data and stratigraphical and geochronological evidence for some high coastal dunes in southern France (Grandjean et al., 2001) and in southeastern Queensland of Australia (Lees, 2006).

Our interpretation of the relatively significant role of the climatic variations in building the giant dunes is supported by geomorphic and sedimentological evidence showing distinct variation in climatic conditions during the late Quaternary in the Badain Jaran and its adjacent regions. The Pleistocene periods of increased rainfall occurred at around 31, 25, and 19 ka BP according to the radiocarbon chronology of the calcareous cementation on the dunes (Yang et al., 2003) and the radiocarbon ages of the high lake level in the inter-dune depressions (Hofmann and Geyh, 1998), and the middle Holocene was the wettest epoch during the Holocene with obvious increase in lake level of many inter-dune lakes in the Badain Jaran (Yang, 2006; Yang et al., 2010a). Such nature of the long-term climate variability in the desert is broadly consistent with the climatic variations inferred from the aeolian sequences in the southern margin of the Badain Jaran (Li et al., 2005) and with the fluctuations recorded in the lacustrine sediments of the lake Juyanze (Juyan Lake) located northwest of the sand sea (Hartmann and Wünnemann, 2009). Although the amount of the annual rainfall during these wetter Quaternary periods is not yet precisely estimated, the studies in other desert regions, however, suggest that doubling from today's value was quite likely. Two cases may be considered as relevant references for this interpretation. In the Qaidam Basin, an arid region located west of the Badain Jaran, the sedimentation rate of the clastic sediments indicates that mean annual rainfall increased to 150–350 mm a^{-1} in the late Quaternary in areas where present mean annual rainfall is <50 mm a^{-1} (Hövermann, 1998). Although it is more distant away, the case of the Arabia offers a more quantitative assessment of the potential amplitude of the increase in rainfall during the pluvial periods in the arid landscape of western Asia. From the speleothem deposition it was concluded that the annual precipitation must have been significantly higher than 300 mm a^{-1} during the Quaternary wetter periods in the southern Arabia where the mean annual precipitation is around 120–170 mm a^{-1} at present (Fleitmann et al., 2011).

The spare vegetation (grasses and shrubs) on the scattered plants on the ridges, maintained by low but sustained annual rainfall (~100 mm; Yang et al., 2010a), also contributes to dune stability. This plant cover helps trap moving sand, and without this limited cover the aeolian sands would be easily eroded and transported. Any future increase of temperature associated with global warming would decrease the precipitation/evaporation (PE) ratio and consequently reduce available moisture and possibly decrease vegetative cover. The sparse vegetation on the dune surface has also experienced severe degradation in the past 60 years primarily due to increases in grazing pressure and more recently due to increased off-road motorized vehicle use. Our analysis of *NDVI* (Normalized Difference Vegetation Index), and *LAI* (Leaf Area Index) data from MODIS (16-Day L3 Global 250 m) between 2000 and 2010 reveals both a weak seasonal cycle and evidence of a decreasing trend in vegetative cover that we attribute to vegetation loss from land use change and possibly from recent climate change.

4. Conclusions

Our studies show that a hilly bedrock landscape, an abundant fluvially-produced sediment supply around the desert margins, complex wind regimes, and stabilization of surfaces produced by a climate alternating between arid and wetter conditions are all of great significance in forming the tallest dunes on Earth. Our findings suggest that the formation processes of such dunes are much more complicated than previously thought and additional factors need to be considered to resolve some of the disputes about the origin and formation mechanisms of tall dunes on Earth. While researchers have primarily focused on wind regimes and sediment properties to explain these dune features, our research suggests that a more comprehensive understanding of dune morphology and height on Earth and other planetary bodies is only possible after careful consideration of topographic features underlying and surrounding the dunes. This is now possible as a result of global coverage of SRTM (Blumberg, 2006; Zandbergen, 2008) and ASTER (Hugenholtz and Barchyn, 2010) digital elevation model data.

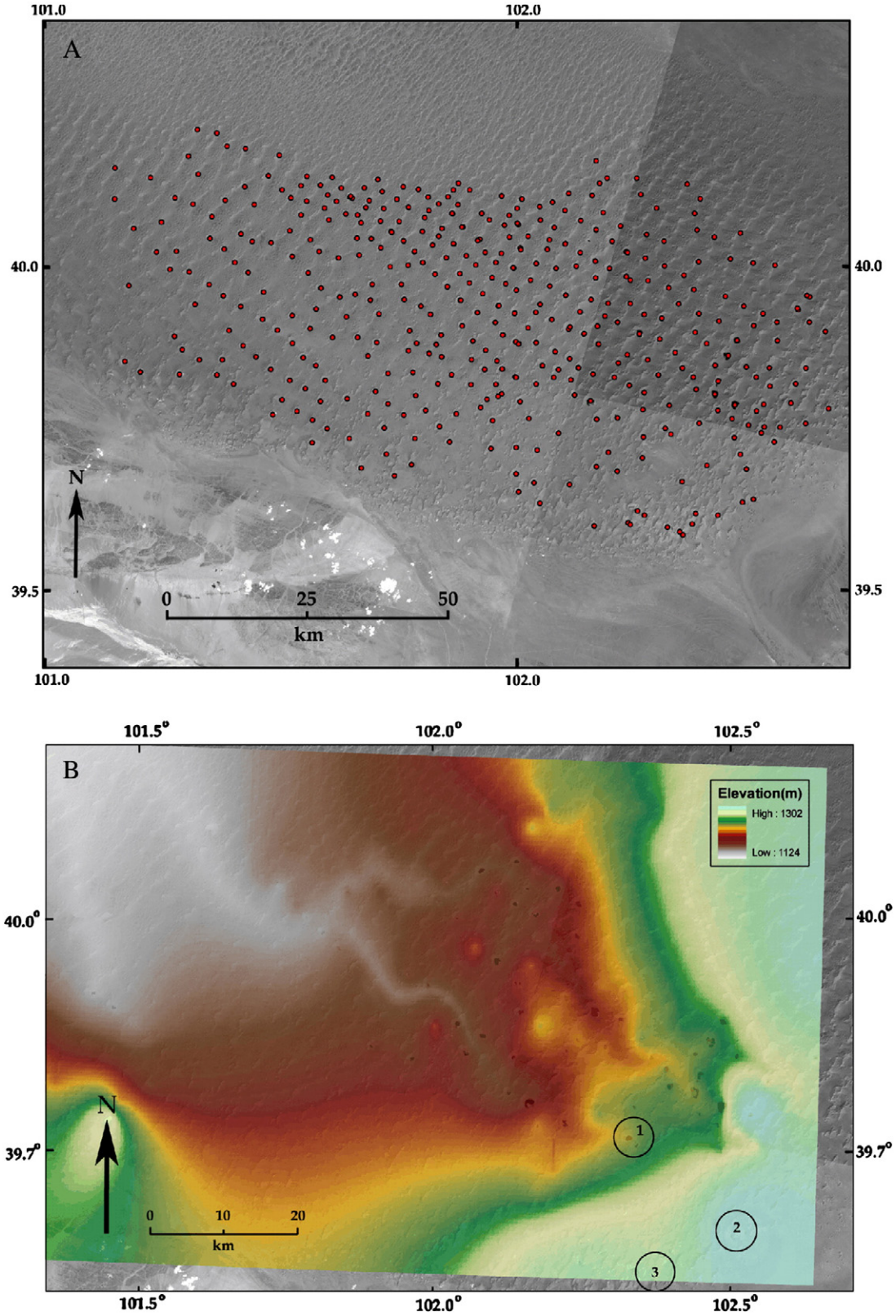

Fig. 6. Topography inferred from the surface DEM. A) Locations of ~350 interdune low points (red dots), extracted from SRTM data. All data was visually checked against Landsat Band 8 (15 m) data and Google Earth imagery to assure that elevation points were located at an interdune low point, usually associated with a lake, marshy area or salt pan. Approximately 10% of the data were rejected because of differences between the two data sets and uncertainty as to whether the SRTM elevation was actually co-located at a topographic low. For reference purposes elevation points and reconstructed surfaces in the figure are projected on a Landsat Band 8, 15 m panchromatic mosaic. B) Subsurface elevation trends. SRTM derived interdune elevation, latitude and longitude locations were converted into an ArcGIS data format and a gridded surface was derived using nearest neighbor interpolation. Data were originally collected prior to the release of the ASTER elevation data set (Hugenholtz and Barchyn, 2010). We assume that this newer, higher resolution dataset will refine but not materially change the results of our analysis. This approach captures an apparent subsurface erosional surface and embedded drainage system (higher elevations are blue and green, and the lowest elevations are white). Areas 1, 2 and 3 correspond to the locations of Figs. 2, 3 and 4, respectively. Area 1 corresponds to the upper portion of a significant subsurface drainage while Areas 2 and 3 are located higher on the buried surface.

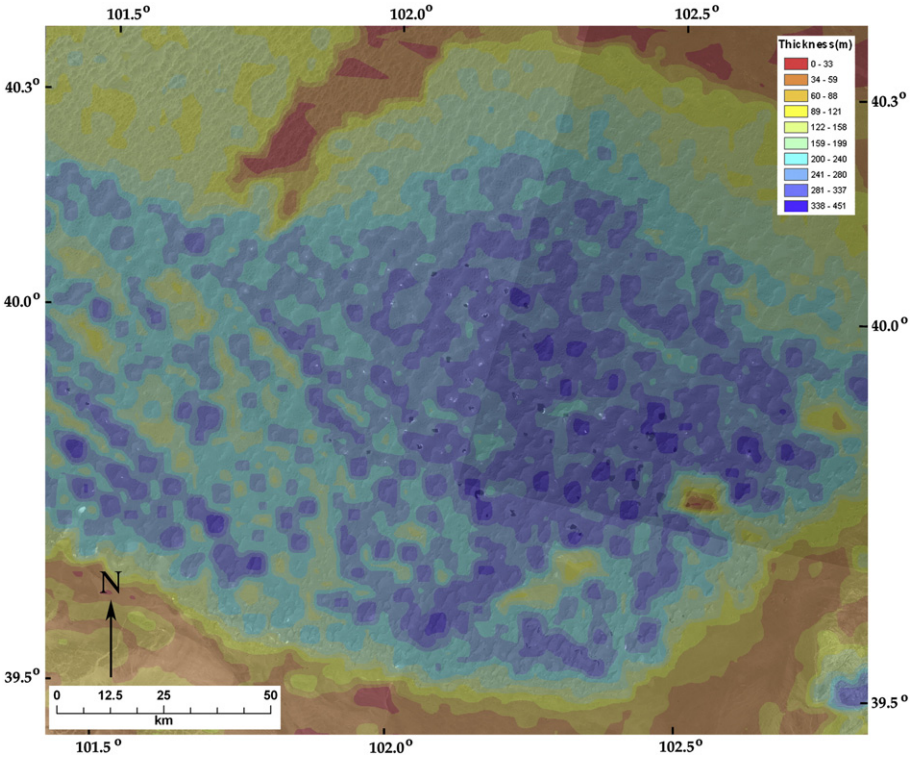

Fig. 7. Variation in sand thickness in the south-central portion of the Badain Jaran Desert based on SRTM elevation differences between the interdune lows and the dune maximum heights. Maximum values of ~350 m are comparable to those suggested by analysis of ASTER data in the Badain Jaran (Hugenholtz and Barchyn, 2010).

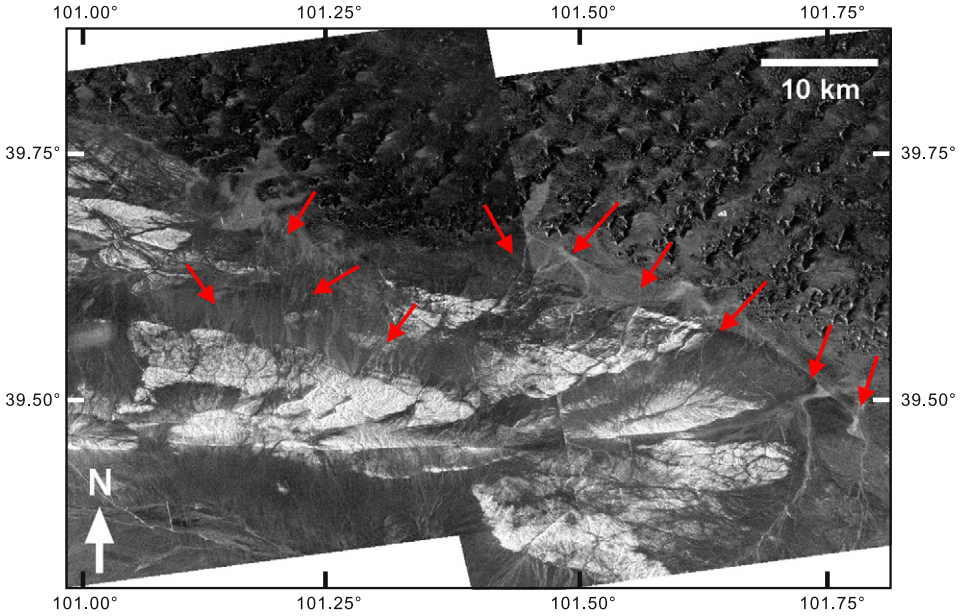

Fig. 8. Radar images of the southern Badain Jaran (for location see Fig. 1). Sediment supply routes from the southern mountains (i.e., the intermittent stream channels) appear as bright linear forms on the radar images (red arrows). The images are from the ALOS/PALSAR instrument, and PALSAR data were provided by JAXA in the framework of the Kyoto & Carbon project (Rosenqvist et al., 2007).

Acknowledgements

The multinational collaborative research was funded by the National Natural Science Foundation of China (grant no. 40930105), the CAS Strategic Priority Research Program (grant no. XDA05120502) and the National Aeronautics and Space Administration of the United States (NASA Earth Science Enterprise to LAS under grants NAG13-03020 and NNS04AB25G). We thank the Chinese Meteorological Agency for providing wind data, the Institute of Geophysics, China Earthquake Administration for technical support, Prof. Changcai Hua and Senior-Ing. Junrang Yang for field assistance and for help in interpreting the gravity data, and Dr. Xinyan Fan for help in interpreting

the wind data. We are very grateful to Prof. Zhenxing Yao and Prof. Tianyao Hao for scientific advices about geophysical methods. Sincere thanks are extended to Prof. Nick Lancaster, Prof. Dirk Goossens, an anonymous reviewer and Editor Prof. Takashi Oguchi for their constructive comments on earlier drafts of this manuscript and for editorial help.

References

Andreotti, B., Fourrière, A., Ould-Kaddour, F., Murray, B., Claudin, P., 2009. Giant aeolian dune size determined by the average depth of the atmospheric boundary layer. Nature 457, 1120–1123.

Annecchione, M., Chouteau, M., Keating, P., 2001. Gravity interpretation of bedrock topography: the case of the Oak Ridges Moraine, southern Ontario, Canada. Journal of Applied Geophysics 47, 63–81.

Bagnold, R., 1941. Physics of Wind-Blown Sand and Desert Dunes. Methuen, London.

Blumberg, D., 2006. Analysis of large aeolian (wind-blown) bedforms using the Shuttle Radar Topography Mission (SRTM) digital elevation data. Remote Sensing of Environment 100, 179–189.

Breed, C.S., Grow, T., 1979. Morphology and distribution of dunes in sand seas observed by remote sensing. In: McKee, E.D. (Ed.), A Study of Global Sand Seas. : Geological Survey Professional Paper, Vol. 1052. U.S. Government Printing Office, Washington, pp. 253–302.

Bullard, J., 1997. A note on the use of the "Fryberger method" for evaluating potential sand transport by wind. Journal of Sedimentary Research 67, 499–501.

Bullard, J., Livingstone, I., 2010. Classics in physical geography revisited — Wasson RJ and Hyde R (1983) Factors determining desert dune types. Nature 304: 337–339. Progress in Physical Geography 34, 857–862.

Burger, H., Sheehan, A., Jones, C., 2006. Introduction to Applied Geophysics: Exploring the Shallow Subsurface. Norton & Company Inc., New York.

Chen, J., Li, L., Wang, J., Barry, D., Sheng, X., Gu, W., Zhao, X., Chen, L., 2004. Groundwater maintains dune landscape. Nature 432, 459–460.

Craddock, R., Hutchinson, M., Stein, J., 2010. Topographical data reveal a buried fluvial landscape in the Simpson Desert, Australia. Australian Journal of Earth Sciences 57, 141–149.

Delgado-Fernandez, I., 2011. Meso-scale modelling of aeolian sediment input to coastal dunes. Geomorphology 130, 230–243.

Dobrin, M.B., 1976. Introduction to Geophysical Prospecting, 3rd ed. McGraw-Hill, New York.

Fleitmann, D., Burns, S., Pekala, M., Mangini, A., Al-Subbary, A., Al-Aowah, M., Kramers, J., Matter, A., 2011. Holocene and Pleistocene pluvial periods in Yemen, southern Arabia. Quaternary Science Reviews 30, 783–787.

Fryberger, S., Dean, G., 1979. Dune forms and wind regime. In: McKee, E. (Ed.), A Study of Global Sand Seas: United States Geological Survey Professional Paper, 1052, pp. 137–169. Washington.

Goossens, D., 1997. Long-term aeolian loess accumulation modelled in the wind tunnel: the Molenberg case (central loess belt, Belgium). Zeitschrift für Geomorphologie 41, 115–129.

Goudie, A., 2002. Great Warm Deserts of the World. Oxford University Press Inc., New York.

Grandjean, G., Paillou, P., Dubois-Fernandez, P., August-Bernex, T., Baghdadi, N., Achache, J., 2001. Subsurface structures detection by combining L-band polarimetric SAR and GPR data: example of the Pyla Dune (France). IEEE Transactions on Geoscience and Remote Sensing 39, 1245–1258.

Hamdi-Nasr, I., Inoubli, M., Salem, A., Tlig, S., Mansouri, A., 2009. Gravity contributions to the understanding of salt tectonics from the Jebel Cheid area (dome zone, Northern Tunisia). Geophysical Prospecting 57, 719–728.

Hammer, S., 1939. Terrain corrections for gravimeter stations. Geophysics 4, 184–194.

Hartmann, K., Wünnemann, B., 2009. Hydrological changes and Holocene climate variations in NW China, inferred from lake sediments of Juyanze palaeolake by factor analyses. Quaternary International 194, 28–44.

Hofmann, J., Geyh, M.A., 1998. Untersuchungen zum ^{14}C-Reservoir Effekt an rezenten und fossilen lakustrinen Sedimenten aus dem Südosten der Badain Jaran Wüste (Innere Mongolei/VR China). Berliner Geographische Abhandlungen 63, 83–98.

Hövermann, J., 1998. Zur Paläoklimatologie Zentralasiens – quantitative Bestimmung von Paläoniederschlag und -temperatur. Petermanns Geographische Mitteilungen 142, 251–257.

Hugenholtz, C., Barchyn, T., 2010. Spatial analysis of sand dunes with a new global topographic dataset: new approaches and opportunities. Earth Surface Processes and Landforms 35, 986–992.

Jäkel, D., 1996. The Badain Jaran Desert: its origin and development. Geowissenschaften 14, 272–274.

Kocurek, G., Lancaster, N., 1999. Aeolian system sediment state: theory and Mojave Desert Kelso dune field example. Sedimentology 46, 505–515.

Lancaster, N., 1995. Geomorphology of Desert Dunes. Routledge, London.

Lancaster, N., 2006. Linear dunes on Titan. Science 312, 702–703.

Lees, B., 2006. Timing and formation of coastal dunes in northern and eastern Australia. Journal of Coastal Research 22, 78–89.

Lennox, D., Carlson, V., 1967. Geophysical exploration for buried valleys in an area north of two hills Alberta. Geophysics 32, 331–362.

Li, B., Gao, Q., Yan, M., Li, Y., Zhong, G., Wen, X., 2005. A recent study on sedimentary sequence of southeastern Badain Jaran Desert since 150 ka BP. Journal of Desert Research 25, 457–465 (in Chinese with English Abstract).

Livingstone, I., Wiggs, G., Weaver, C., 2006. Geomorphology of desert sand dunes: a review of recent progress. Earth-Science Reviews 80, 239–257.

Lorenz, R.D., Radebaugh, J., 2009. Global pattern of Titan's dunes: radar survey from the Cassini prime mission. Geophysical Research Letters 36, L03202.

Narteau, C., Zhang, D., Rozier, O., Claudin, P., 2009. Setting the length and time scales of a cellular automaton dune model from the analysis of superimposed bed forms. Journal of Geophysical Research 114, F03006.

Parteli, E.J.R., Durán, O., Tsoar, H., Schwämmle, V., Hermann, H., 2009. Dune formation under bimodal winds. PNAS 106, 22,085–22,089.

Richthofen, F., 1877. China: Ergebnisse Eigener Reisen und darauf Gegründeter Studien. Erster Band. Reimer, Berlin.

Rosenqvist, A., Shimada, M., Ito, N., Watanabe, M., 2007. ALOS PALSAR: a pathfinder mission for global-scale monitoring of the environment. IEEE Transactions on Geoscience and Remote Sensing 45, 3307–3316.

Rubin, D.M., Hesp, P.A., 2009. Multiple origins of linear dunes on Earth and Titan. Nature Geoscience 2, 653–658.

Weissmann, G.S., Hartley, A.J., Nichols, G., Scuderi, L.A., Olson, M., Buehler, H., Banteah, R., 2010. Fluvial form in modern continental sedimentary basins: Distributive Fluvial System. Geology 38, 39–42.

Yang, X., 1991. Geomorphologische Untersuchungen in Trockenräumen NW-Chinas unter besonderer Berücksichtigung von Badanjilin und Takelamagan. Göttinger Geographische Abhandlungen 96, 1–124.

Yang, X., 2006. Chemistry and late Quaternary evolution of ground and surface waters in the area of Yabulai Mountains, western Inner Mongolia, China. Catena 66, 135–144.

Yang, X., Liu, T., Xiao, H., 2003. Evolution of megadunes and lakes in the Badain Jaran Desert, Inner Mongolia, China during the last 31000 years. Quaternary International 104, 99–112.

Yang, X., Ma, N., Dong, J., Zhu, B., Xu, B., Ma, Z., Liu, J., 2010a. Recharge to the inter-dune lakes and Holocene climatic changes in the Badain Jaran Desert, western China. Quaternary Research 73, 10–19.

Yang, X., Liu, T., Yuan, B., 2010b. The Loess Plateau of China: aeolian sedimentation and fluvial erosion, both with superlative rates. In: Migon, P. (Ed.), Geomorphological Landscapes of the World. Springer, Dordrecht, pp. 275–282.

Yao, C., 2009. MASK 2000 — A Computer Program for Geophysical Modeling (Revised Version). China University of Geosciences, Beijing.

Zandbergen, P., 2008. Applications of Shuttle Radar Topography Mission elevation data. Geography Compass 2 (5), 1404–1431.

Zhang, D., Narteau, C., Rozier, O., 2010. Morphodynamics of barchan and transverse dunes using a cellular automaton model. Journal of Geophysical Research 115, F03041.

Zhu, Z., Wu, Z., Liu, S., Di, X., 1980. An Outline of Chinese Deserts. Science Press, Beijing. (in Chinese).

Zhu, Z., Chen, Z., Wu, Z., Li, J., Li, B., Wu, G., 1981. Study on the Geomorphology of Wind-drift Sands in the Taklamakan Desert. Science Press, Beijing. (in Chinese).

Zimbelman, J., 2010. Transverse aeolian ridges on Mars: first results from HiRISE images. Geomorphology 121, 22–29.